

Investigation of Wheel Squeal Characteristics using a Rolling Contact Two Disk Test Rig

Meehan P.A.¹, Bellette P.¹, Liu X.¹, Milne C.¹ & Anderson D.²

¹The University of Queensland & CRC for Rail Innovation, Brisbane, Australia

²RailCorp, New South Wales, Australia

SUMMARY

This paper investigates the prediction of fundamental squeal behaviour on a two disk rolling contact test rig based on theoretical, numerical and experimental testing. It is focused on the identification of the squeal modes of vibration and nonlinear contact mechanical effects appearing in the sound spectra. To investigate and identify the dominant squeal modes, a theoretical calculation based on a simplified geometry of the test rig disk as well as finite element analysis results of the full geometry was performed. Full comparison of these results was then made with experimental impact hammer tests performed on the test rig under static conditions and actual squeal noise frequency measurements under rolling conditions confirming the utility of the theoretical and experimental methods for wheel squeal frequency prediction. In addition, the occurrence of low frequency harmonics in the noise spectra was identified and investigated using classical squeal modelling coupled with nonlinear contact mechanics. A numerical analysis of the contact dynamics was performed, to reveal model predicted harmonics correlating with those found in the sound spectra. The effect of speed on the occurrence and characteristics of the harmonics was also investigated both theoretically and experimentally to reveal further insight into the nonlinear contact mechanical effects on squeal noise spectra.

1. INTRODUCTION

“Wheel Squeal” describes the high pitched tonal noise a train’s wheels can make as they negotiate a curve (corner) of a railway line. This phenomenon has plagued the railway industry for many years and is becoming more critical as railway usage increases and subjective human noise tolerance decreases. Although much research insight has been obtained into the mechanisms of squeal over the past decade the occurrences of wheel squeal still appear unpredictable as it is sensitive to a wide range of parameters that naturally vary in the field. In order to investigate this phenomenon further under more controlled conditions, a two disk rolling contact machine has been developed to allow much more readily available measurements and conditions to be investigated. It comprises two steel wheels of different diameters driven by vector controlled motors under tractive rolling contact. An angle of attack may be imposed between the disks to investigate wheel squeal under cornering/curving conditions.

Much modelling of wheel squeal has been performed particularly following the renowned works of Rudd[1] and review by Remington[2] and Thomson et al[3] in which the fundamental mechanism due to lateral creepage was more or less consolidated. Curve squeal is generally thought to originate from the unstable vibratory response of a railway wheel when subject to large

creep forces whilst negotiating corners. Present consensus from the literature is that the unstable excitation of the squealing wheel originates from a lateral ‘stick-slip’ mechanism in the contact region analogous to the bowing of a violin string. Pure tone components of squeal, in the range 600 – 10,000 Hz, are generally related to wheel natural frequencies that correspond to the out-of-plane wheel bending (or axial) modes.

Various theories, although much simplified, have evolved over the years to describe the lateral traction ratio (lateral tangential force Q_y , divided by the normal force N) and lateral creepage (\approx angle of attack) conditions during the excitation of a railway wheel in curves [13,4] as shown in Figure 1. Referring to Figure 1, under tractive rolling contact, traction first grows approximately proportionally with creepage (see a)), as the area of adhesion (slip) within the contact region decreases (increases).

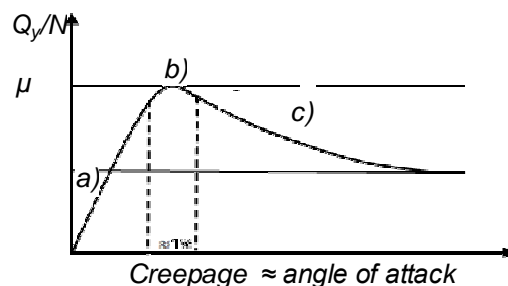


Figure 1. Traction/creepage characteristic of railway wheel-rail contact. a) region of slip/adhesion, b) point at which full sliding first occurs and c) negative slope region of increased sliding causing negative damping of creep oscillations.

For further increasing creepage, the traction reaches a maximum value equal to the static coefficient of friction, μ at b). Past this point there is insufficient friction within the contact region to prevent full sliding (no adhesion within the contact). The quasistatic creep force then shows a falling (negative slope) characteristic with the lateral force reducing with increasing creepage once the contact is in full sliding (see c)). The friction coefficient and shape and slope of the traction/creepage curve is effected by the so-called third body of the contact; an interfacial layer consisting of any lubricants, contaminants and material generated as a result of the contact interaction [5]. The negative slope in the creep curve at c) can be shown to be associated with negative damping of creep oscillations and hence squeal instability. Nearly all squeal models are based on this same mechanism: An angle of attack is imposed on the wheels by the bogie dynamics in the curve—this means the wheel slides laterally across the rail in addition to rolling—this is associated with a high lateral “traction-creep” force leading to self-excited “stick-slip” oscillations, which in turn excite wheel vibrations and radiated sound. The main differences between the models lie in details in the modelling of wheel/rail mechanical impedances (analytical [6,7,8,9,10], FEM [11,12,13]), vertical dynamics [12,13], contact forces and wheel sound radiation [11,12,13]. Some have also included wheel/rail roughness or wheel rotation effects [9,10]. Recently, a transient analysis of the lateral creepage of the wheel was performed to account for nonlinearities of friction forces and resultant excited wheel modes appeared to match field observations better [14].

Much recent research has also been focussed upon experimental validation of model predicted conditions under which squeal occurs and the effect of friction modifiers [15] on the phenomena. Recent predictive modelling includes that of [13,16] which include detailed representation of the dynamic behaviour of the wheel and rail and creepage in the saturated region. Twin disk and bogie testrigs have been utilised for validation under controlled environments [17]. Experimental results reported on the rolling contact force conditions during squeal include those by de Beer et al. [13], Monk-Steel et al. [16] and Koch et al [18]. In Monk-Steel et al. [16] the inclusion of longitudinal creep was shown to reduce the lateral creep force and thereby change the slope of the friction curve. This leads to a lower incidence of squeal in the presence of longitudinal creep, and

an increase in the threshold of lateral creepage necessary for squeal. In Koch et al [18], measurements were carried out on a 1/4 scale test rig including a mono-block wheelset, and tests of anti-squealing solutions. A relation between noise level, rolling speed and angle of attack was confirmed experimentally and the average friction coefficient as a function of lateral creep was measured/inferred in dry conditions and with water. In [17] novel instrumentation directly on twin disc wheels close to the contact patch was used to obtain more direct measurements of lateral force to provide some validation of existing predictive models although the presence of a third body in the contact appears to affect the reliability of the testrig results. In [15] friction modifiers were shown to cause substantial (~12 dB) noise reductions associated with top-of-rail squeal and flanging noise at range of European mass transit sites. Despite these considerable efforts, there has been little success in closely correlating model predictions with characteristically “noisy” experimental measurements and observations of wheel squeal occurrences. In particular, experimental evidence and explanation of nonlinear effects of the contact mechanics on squeal noise spectra have not been identified previously to the authors knowledge.

The present research investigates the prediction of fundamental squeal characteristics on a two disk rolling contact testrig including the identification of the squeal modes of vibration and nonlinear contact mechanical effects appearing in the sound spectra. The major contributions include:

1. Comprehensive theoretical and experimental identification and prediction of the dominant modes of wheel squeal and corresponding validation with noise spectra measurements from a squealing testrig.
2. Theoretical identification and prediction of nonlinear contact mechanical based harmonics and their dependence on speed and corresponding validation with noise spectra measurements from a squealing testrig.

This paper will first describe the testrig and methodology used for squeal investigation. Subsequently, descriptions of the methods for prediction of the dominant squeal frequencies and comparisons with actual measurements are provided. An investigation into the occurrence of low frequency harmonics in the noise spectra is then provided using classical squeal modelling coupled with nonlinear contact mechanics before conclusions are drawn.

2. Two disk rolling contact test rig

An outline of the test rig experimental equipment, its setup and the methodology used is provided in the following subsections.

2.1 Description of test rig

The use of roller rigs has a long history in the study of railway dynamics and contact mechanics. They can be either full size, or scaled to allow for efficient and cost effective study, provided certain scaling conditions are met to ensure accurate simulation of the full scale system [19]. The UQ (University of Queensland) Rail Corrugation Test Rig consists of two steel disks of differing radii in rolling contact to achieve maximum stress conditions similar to field conditions. The material of the wheel and lower disk is cast steel of chemical composition similar to the wheel/rail steels. A summary of the important test rig parameters can be found in table 1.

Table 1 – Test Rig Parameters

Description	Value
Lower Disk Radii of curvature (longitudinal, lateral)	0.213 m, 0.300 m
Upper Disk Radii of curvature (longitudinal, lateral)	0.085 m, 0.040 m
Normal Force Range (P_0)	0 - 2000 N (400N)
Tangential Load Range (Q_0)	0 - 1000 N
Friction Coefficient (μ)	0.45 (Dry), 0.15 (Friction Mod.)
Typical Lower Disk Rolling Contact Velocity Range	0 – 1200 RPM 0 - 26.8 m/s
Disk Material	Cast Steel (0.71%C, 0.46%Si, 0.85%Mn, 0.05%Cr, 0.02% Ni, 0.01% Mo, 0.02% S, 0.02% P)
Yield Strength	420 MPa
Density (ρ)	7800 kg/m ³
Poisson's Ratio (ν)	0.28
Wear Coefficient, k_0	1.6×10^{-9} kg/Nm (Dry), 0.34×10^{-9} kg/Nm (Friction Mod.)
Angle of attack,	0-50 mrad (24.3mrad)

The normal force, braking traction and lower disk speed are controllable parameters. The test rig is instrumented to obtain measurements of the normal force through strain gauges on the main springs, disk speeds through position encoders (RP 6010 with 1/1000 resolution) on the drive shafts. The traction force can be inferred from the torque measured via strain gauges on the drive shafts, the longitudinal profile is measured via a proximity probe (MicroPROX@_3300 REBAM, with precision less than 0.1 μm and repeatability of 0.43 μm) and disk temperature recordings can also be taken (Raytek with $\pm 1\%$ in accuracy and $\pm 0.5\%$ in repeatability). Data is acquired through a 3B Series Subsystem and transferred to a DAQ Card (6024E) which provides digital input to a laptop. The speed, torque, normal force,

temperature and lower disk profile height measurements are displayed and logged using a MATLAB based software interface. The test rig setup can be seen in Figure 2.

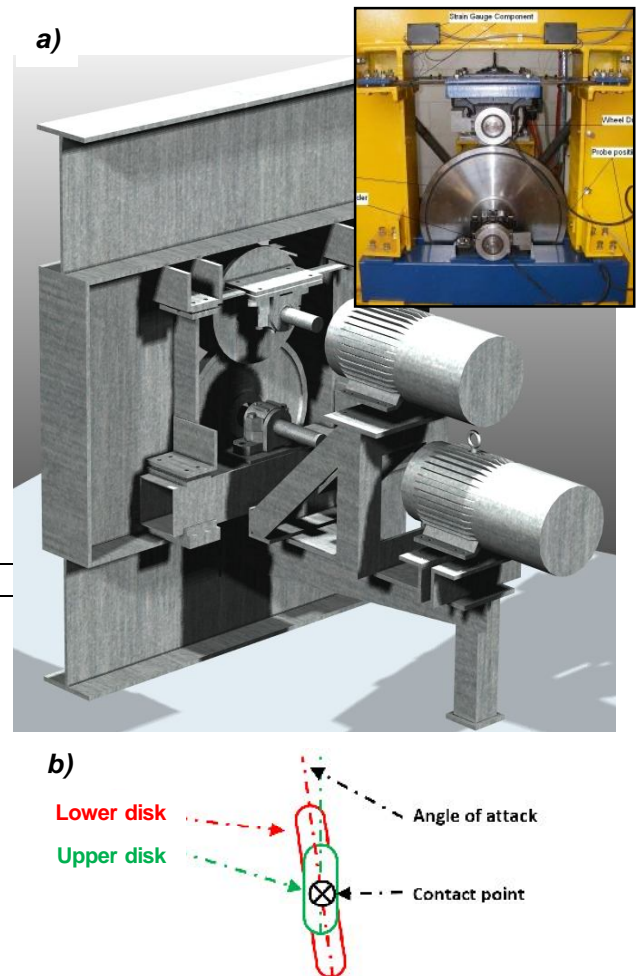


Figure 2. Two Disk Rolling Contact Test Rig; Main components b) Angle of attack

The rotating axes of the Two Disk Rolling Contact Test Rig may be misaligned to introduce an angle of attack to the two wheels, to simulate squeal noise. The angle of attack is achieved by rotating the lower disk and motor through an angle (about the vertical axis) to the frame as shown in Figure 2 b).

2.2 Experimental methodology for test rig squeal

Prior to testing the disk profiles were machined to the correct geometry and the contacting surfaces of both the upper and lower disks were cleaned with ethyl alcohol. The lower disk was set at an angle of about 24.3 milliradian to the test rig frame (and upper disk), the constant torque motor was set to zero torque and there was $400\text{N} \pm 20\%$ of normal force applied between the wheels via careful adjustment of shims under the leaf springs. Under these conditions, the contact ellipse was approximately 1 mm along both axes. The sound of the test rig was recorded for speeds of the lower

disk of 100 to 700 RPM in 100 RPM increments. In this process the torque was approximately zero. While running, the speeds of the two disks, the torques on the shafts and the contact force were regularly recorded to ensure the tests had consistent parameter values. It was found that during tests the torque and slip between the two disks had to be carefully controlled to avoid any large transient increases in slip that may alter the contact geometry and surface conditions by the rapid wear rates.

The sound pressure levels of the test rigsquealing were recorded using a microphone placed adjacent to (5cm away from) the lower disk, a conditioning amplifier and an analogue digital converter (ADC). The signal from the amplifier was sent to an analogue to digital converter and then to a laptop via USB. The program used on the laptop to record the signal was Labview's Signal Express 3.0 by National Instruments. The sound was recorded each time for 2 seconds, twice for each increment at a sample rate of 8000Hz. The voltage signal was transformed into the frequency domain and rescaled in decibels using a Matlab program with the reference pressure set at 20µPa RMS. The results from these recordings are provided in section 3.4.

In the subsequent sections 3 and 4, the contributions of the resonances of the lower disk (section 3) and the nonlinear rolling contact mechanics (section 4) to the testrig squeal noise under an angle of attack is investigated.

3. Prediction of Wheel Modes of Vibration

Three methods of prediction of the wheel modes of vibration were performed in order to achieve a comprehensive evaluation of the precision and usefulness of theoretical, numerical and experimental methods for squeal frequency prediction. Firstly an analytical formula for the natural modes of vibration in a disk was used to determine that in the large (lower) disk. The natural frequencies of the large disk and corresponding modeshapes were also acquired using Finite Element Analysis (FEA). Subsequently, experimental modal analysis was used to compare with the theoretical results. Note that the large disk typically represents the rail in previous corrugation studies [20] however in the present investigation, squeal is found to emanate from the larger disk due to a lower transverse stiffness and larger propagational surface area. Subsections 3.1-4 describe the methodologies used and 3.5 provides the results comparison with actual testrig squeal measurements and discussion.

3.1 Analytical Method

The theoretical modes of vibration of the lower disk may be analytically determined by simplifying its geometry to an annular plate with free and fixed boundary conditions around the outer and inner circumferences, respectively (see[21]). In particular, if it is assumed that the lower disk is a thin, flat, uniform thickness plate of linear elastic, homogeneous, isotropic material with small deformations in comparison with the thickness of the plate and that the effects of shear deformation, rotary inertia and/or gyroscopic effects under rolling are negligible, the lateral modal frequencies of the disk may be estimated analytically as,

$$f_{ij} = \frac{\lambda_{ij}^2}{2\pi a^2} \left[\frac{Eh^3}{12\gamma(1-\nu^2)} \right]^{1/2}; i, j = 0, 1, 2, \dots (1)$$

where f is the modal frequency (Hz), λ the dimensionless frequency parameter, a and b the outer and inner radii, h the plate thickness; i and j the number of nodal diameters and circles in the mode shape (see Table 2), and E, γ and ν the modulus of elasticity, mass per unit area and Poisson's ratio of plate, respectively. Eq. (1) is adapted from the exact analysis of an annulus by Vogel and Skinner [22], using the results expressed in a form using the flexural rigidity explicitly, as in Rao and Prasad [23]. Using Eq. (1) the lowest lateral modal frequencies and shapes were calculated as shown in Table 2 using the disk parameters defined in the last row.

Table 2. Values used in equation (1) and calculated natural frequency

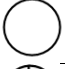
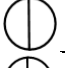
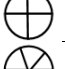

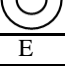
i	j	λ^2	f (Hz)	Mode Shapes	
0	0	4.87	394		
1	0	4	323		
2	0	6.2	500		
3	0	12.6	1017		
0	1	29.876	2412		
a	b	h	γ	N	E
0.2125m	0.0325m	0.015m	117.75kg/m ²	0.3	200GPa

Table 2 highlights that the vibration of a wheel is characterised by mode shapes of nodal circle/s and nodal diameter/s. For comparison with these results, and to ascertain which ones are dominant with squeal, numerical and experimental measurements were performed as detailed in the subsequent sections.

3.2 Numerical Method using FE Analysis

Prediction of the lateral modes of the lower disk was also performed using Finite Element Analysis based on a more accurate geometrical representation of the lower disk specified in Solid

Edge/CAD. The typical 1mm radius blend was not included in the representation for meshing simplicity. The CAD representation (.igs file) was imported into Strand 7 and then meshed with 3 different meshes (5%, 3% and 2% maximum mesh edge length, i.e. 5%, 3% and 2% of the largest dimension of the model) to confirm convergence of an accurate result for the lower natural frequencies of the wheel. The object was constrained by fixing the inside surface from movement in all 6 directions (linear and rotation). The mesh style used was a Tri6 surface mesh and quadratic elements for the solid mesh. The natural frequency solver was run to get the 20 lowest natural frequencies of the lower disk. Figure 3a) shows the wheel as meshed with a 5% maximum mesh edge length in the undeformed shape.

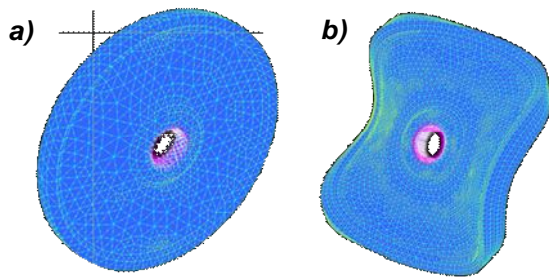


Figure 3. Lower disk FE; a) Undeformed (5%) b) modeshape for 1134Hz (2%); maximum mesh edge length indicated in (a).

Figure 3 b) shows the modeshape for the natural mode at 1134Hz with 3 nodal diameters and no circles (i=3, j=0) corresponding well to the analytical results in Table 2. Detailed results are presented in section 3.4. All modes were characterised by lateral vibrations except for two radial modes at frequencies of 1164 and 3403Hz. Generally only lateral vibration of the lower disk would be expected to cause squeal noise (larger surface area), so the radial modes were not expected to be associated with squeal. Further discussion of the finite element results is provided following the experimental testing for comparison.

3.3 Experimental Method via Impact Hammer Testing

In order to determine the natural frequencies of lower disk experimentally under static conditions, impact hammer tests were performed. These are a type of modal test where an instrumented impact hammer is used to excite an object in order to determine its natural frequencies, modal damping ratios and modal shapes based on precise measurements of the input excitation and output vibrations. Three different impact hammer tests were carried out on the lower disk while it was in the test rig to find its lateral receptance at various positions on the wheel for accelerometer 2 as shown in Figure 4. PCB types 086D05 and 480B21 ICP modally tuned impact hammer with hard tip and signal conditioner was used, respectively to determine the lower disk receptance (spectrum of

dynamic deflection for a given force at each frequency). For these tests the upper disk was jacked up so as not to contact the lower disk, so vibrations of the lower disk were isolated from the upper disk. The two magnetically mounted 100mV/G ICP PCB accelerometers were placed in the positions shown in Figure 4.

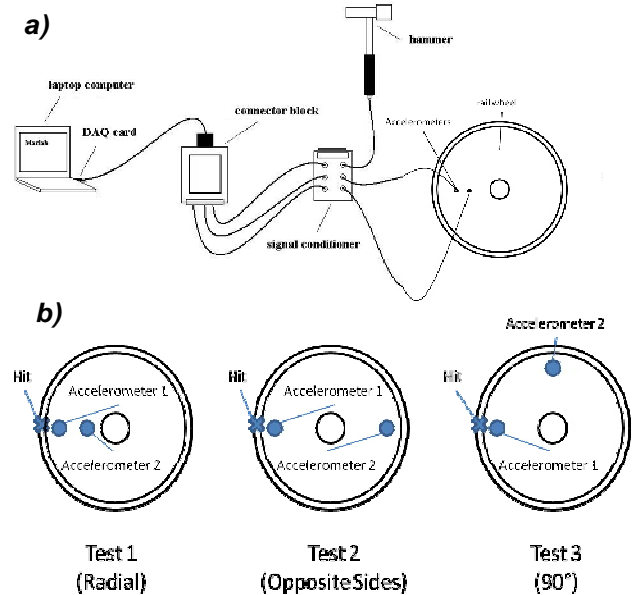


Figure 4. a) Experimental layout of modal impact hammer testing and b) approximate positions of accelerometers and impact for three tests.

Detailed results are presented in section 3.4, however as an example, the results of the first test are shown in Figure 5. In particular, the receptance at accelerometer 1 position is shown with modal peaks at 127, 531, 1138 and 2046 Hz.

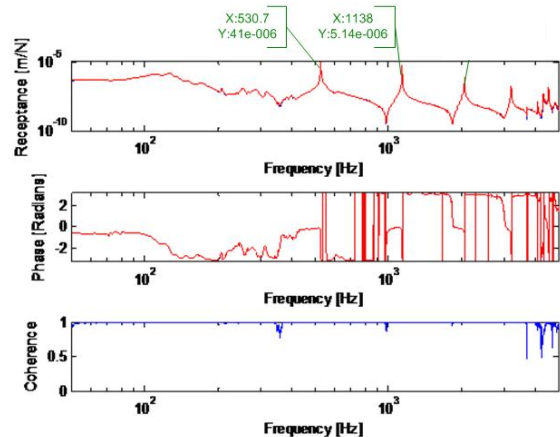


Figure 5. Results of the first impact hammer test for accelerometer 1

Referring to Figure 5 the Coherence was high (≈ 1) for the range of frequencies mentioned, indicating the noise contamination was acceptably low. In the receptance graphs there was also an unexpected peak at 126Hz. It is likely from the results of the different impact hammer tests that this peak is due to movement of the lower shaft in its bearings. Also used are the half power points (roughly $1/\sqrt{2}$

times the peak amplitude) at 119.3 and 130.7 Hz used in the calculations for the numerical analysis of the contact dynamics in section 4.

3.4 Comparative Results and discussion

Measurements of sound spectrum from the testrig during squeal occurrences (as described in section 2) were used to compare with the predicted squeal frequencies from the analytical, numerical and experimental methods described in sections 3.1-3. The squealing testrig sound spectra for two illustrative speeds are shown in Figure 6 to highlight the behaviour of the sound spectrum as the RPM increases.

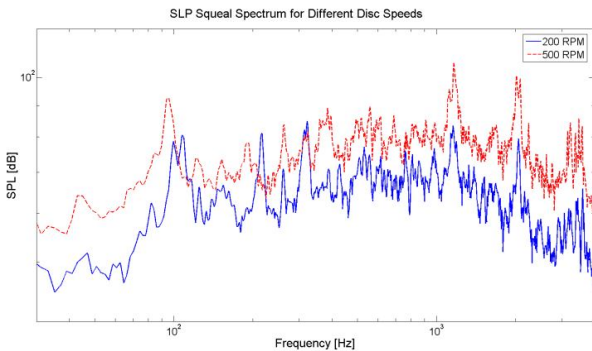


Figure 6. Testrig Squeal Sound Spectra for tests at 200 and 500 RPM

Referring to this figure, there are several resonant peaks evident at various frequencies distinct from the background noise typical of wheel-rail rolling contact. In particular, there are definite peaks at 107, 217, 322, 1160, 2049 and 3599 Hz for the 200 RPM spectrum and at about 95, 385, 559, 1164, 2026, and 3489 Hz for the 500 RPM spectrum. The spectra for 100 RPM had no distinct peaks. The peaks at various frequencies seem generally

to increase in value as the RPM is increased, and some new peaks appear. However some peaks (like the 217 and 322 Hz peaks for 200 RPM run 1) seem to disappear as the RPM is increased. The 107 Hz frequency seems to split into two different peaks at 200 RPM. This may be due to the fact that there are two bearings holding the lower shaft to the frame, and each one reacts slightly differently (two different modes of vibration) at different speeds.

Table 3 summarises the comprehensive comparison of the peaks in the sound spectra for both 200 and 500 RPM runs with the theoretical and experimental predictions of the transverse natural modes of vibration. It can be seen that the peaks in the sound spectra compare well to the predicted modal frequencies from the analytical, numerical (FEA) and impact hammer tests as shown in the table. This provides strong evidence that the squeal noise is associated with the transverse vibration modes of the larger lower disk. In particular, the dominant modes appear to be the third nodal diameter mode at 1162 Hz as depicted in Figure 3 b) followed by the second and fourth at 559 and 2049 Hz, respectively (depending on speed). This is in agreement with the frequencies and magnitudes found in the receptances of the impact hammer tests. In particular, the dominance of the impact receptance peaks at 530, 1138 and 2046 Hz corresponds to that found in the SPL spectra during running. The change in dominance of these three modes at different speeds is likely due to the boundary/damping effect of which is likely to affect these lateral modes differently as a function of nodal wavelengths, speed and modal frequency. Similarly it is likely that the contact patch damped the lateral 391 Hz mode (single nodal diameter) during rolling and hence eliminating evidence of it

Table 3. Natural Modes of Vibration Comparison of analytical, numerical (FEA) and experimental predictions with measured testrig squeal sound spectra.

Natural Frequency (Analytical) (Hz)	Mode Shapes (Analytical)	Natural Frequency (FEA Strand 2% Mesh) (Hz)	Mode Shapes (FEA Strand 2% Mesh) (Hz)	Natural Frequency Impact hammer Receptance (Acc.1, Test 1)		Peaks in testrig sound spectrum for 200RPM run 1		Peaks in testrig sound spectrum of 500RPM run 2	
				Frequency (Hz)	Ampl (µm/N)	Frequency (Hz)	SPL (dB)	Frequency (Hz)	SPL (dB)
				120-130	1-1.4	107	87	96	98
						217	84		
						322	88		
323		391						385	94
500		542		531	8.4			559	95
1017		1134		1138	5.1	1160	90	1162	111
		2026		2046	0.7	2049	91	2022	107
2412		2544				2493	68	2428	83
		3403				3599	78	3489	92

in the squeal SPL spectrum. Table 3 also highlights, that the modal frequencies are well predicted by the analytical and numerical FEA prediction methods with errors under 10%. Compared with the corresponding frequencies from the FEA method in the table 3, the analytical results are slightly lower. This is most likely due to the rim thickness not being accounted for in the analytical model causing an artificially lower transverse stiffness. The 217 and 322 Hz peaks in the spectrum for 200RPM run 1 are thought to be harmonics from the contact dynamics, as investigated and discussed in the next section.

4. Prediction of Effects of Contact Mechanics on Squeal Spectra

The spectra of the sound of the test rig running at 200 and 300 RPM showed peaks at about 200 and 300 Hz that disappeared at higher speeds and were also not identifiable in the theoretical or experimental predictions. This section investigates the possibility that this speed dependent, nonlinear, peak phenomena may arise due to the rolling contact dynamics of the two wheels in the test rig. In particular, classical squeal modelling coupled with nonlinear contact mechanics is first developed in section 4.1 before simulated results and insight gained regarding this phenomena is provided in section 4.2.

4.1 Modelling

A squeal model was developed using a single degree of freedom description of the dominant lateral wheel squeal mode coupled with a nonlinear lateral creep model. The modal lateral squeal vibration may be described by,

$$(2)$$

where m is a mass, c is the damping coefficient, k is the stiffness, Q is a forcing function and ζ is creep. Q is obtained from [24,25], where the nonlinear traction/creep equations are,

$$w < 1, (3)$$

$$\geq 1 (4)$$

where the coefficient of friction is given by,

$$(5)$$

where μ_0 is the reference coefficient of friction, A and B are constants determined by the shape of the creep curve, P is the normal force in the contact and the non-dimensional creep parameter w is defined as,

$$(6)$$

The constant C in (5) is determined by the shape of the creep curve. The formula for Q is an empirical formula designed to fit experimental data, in which the equation for μ is the similar to Polach's equation, except (8) has a $(w-1)$ term

instead of w [24, 25]. A graph of the creep curve used in the numerical analysis is shown in Figure 7 ($A = 2/3$, $B = 0.1$, $C = (1/0.005)$, $\mu_0 = 0.45$ for typical contact with steel wheels (see [25]).

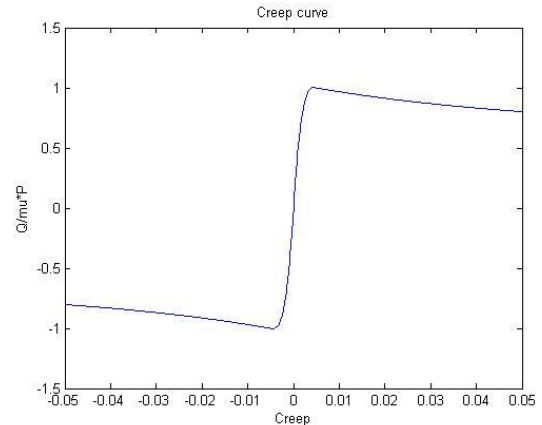


Figure 7. Creep curve used in the numerical analysis for the contact dynamics

It is noted that here $A = \mu_0/\mu_\infty$ where μ_∞ is the coefficient of friction at infinite creep and that C is the inverse of the critical creep, that is where the creep curve peaks [24, 25]. The creep is calculated from the following [26]:

$$, \quad - \quad (7)$$

where v is linear velocity with respect to the point of contact, Ω is the angular velocity with respect to the point of contact, the subscripts m, L and U refer to the mean velocity and lower and upper disks respectively and x, y and z refer to directions as described in Figure 8.

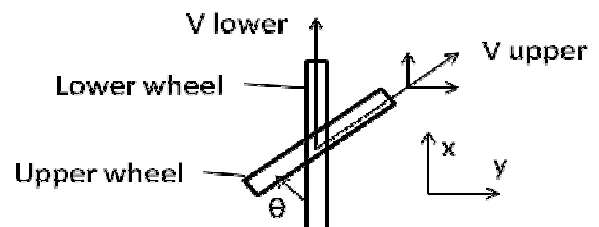


Figure 8. Test rig angle of attack definition

Figure 8 also defines the test rig angle of attack θ . Under the assumptions that the torque between the disks is negligible (set to 0) and the angle of attack is small (ie $\theta \ll 1$ rad), (7) reduces to,

$$- (8)$$

where the subscript y refers to lateral creepage.

4.2 Results

Numerical simulations were performed by integration of the equations of motion in 4.1, using the function "ode45" in Matlab to simulate the movement of the lower disk at the contact. "ode45" is a variable step ordinary differential equation solver based on an explicit Runge-Kutta formula.

Simulations were run over the time interval of 0 to 1 second in increments of 1×10^{-5} s, and with the initial conditions of $y = 0$ and $\dot{y} = 0$. A standard Fast Fourier Transformation function in Matlab was then used to obtain a spectrum of the frequency of motion of the lower testrig disk. The following values are used for the various variables in the program unless otherwise stated: $\theta = 0.025$, $P = 400$ N, $\mu_0 = 0.45$, $C = (1/0.005)$, $A = 2/3$, $B = 0.1$. The values for m , k and c are calculated as follows: a modal mass m was estimated based on the mode shape/FE simulations; $k = m \omega_n^2$ and $c = 2\zeta_{DR}\omega_n m$ where ζ_{DR} is the damping ratio obtained from the quality factor [8] as per equation (9),

$$\zeta_{DR} = \frac{\omega_1 - \omega_2}{2\omega_n} \quad (9)$$

where the angular frequencies ω_1 and ω_2 corresponding to the half power points. As such, the dynamic parameters for the 107Hz mode were $m = 1.305$ kg, $k = 590024$ N/m, $c = 93.95$ Ns/m. For the 1138Hz mode, the dynamic parameters become $m = 0.223$ kg, $k = 1.14 \times 10^7$ N/m, $c = 14.35$ Ns/m.

Fig. 12 shows the FFT spectrum of wheel lateral vibration produced at two different rolling speeds for the 107Hz mode to highlight the effect of the nonlinear contact mechanics.

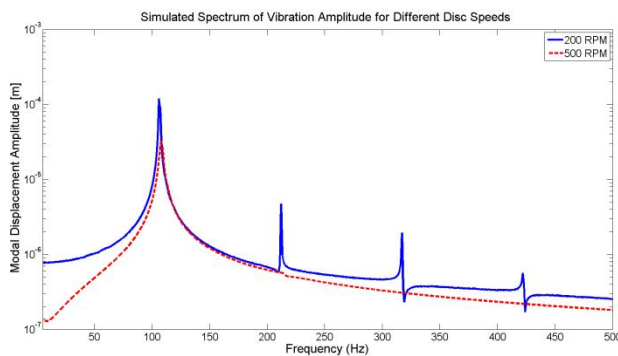


Figure 9. Simulated lower disk vibration spectra using the 107Hz mode during squeal at 200 and 500 RPM.

It can be seen from Figure 9 that at both speeds there is a dominant peak at 107Hz corresponding to the lateral mode of vibration simulated but for the lower speed at 200RPM there are more peaks at regular intervals of approximately 107Hz apart i.e. harmonics of the mode. This appears to correspond well to the harmonics at 217 and 322 Hz visible in the measured testrig sound spectra (Figure 6) at the same speed. In addition, at 500RPM it can be clearly seen in Figures 6 and 8 respectively, that the same harmonics have been substantially reduced/eliminated. It is interesting to note that the amplitude of the peak at the fundamental frequency has also reduced slightly indicating lower overall squeal vibration amplitude. A similar speed dependence on the existence and amplitude of harmonics for higher frequencies including the dominant squeal modes (ie 1137Hz) was also found. Since the dominant squeal lateral

modes are harmonics (multiples) of each other, this would tend to suggest that the same mechanism may be underlying the existence and varying dominance of the dominant lateral wheel squeal modes with speed (ie see Table 3). This should be investigated further with a fully coupled nonlinear FE model.

Insight into the cause of this speed dependent appearance and dominance of harmonics may be obtained by focussing attention on the creep dynamical behaviour at different speeds. In particular, the creepage and traction variations for different speeds for the 1137Hz squeal mode was plotted in Figure 10

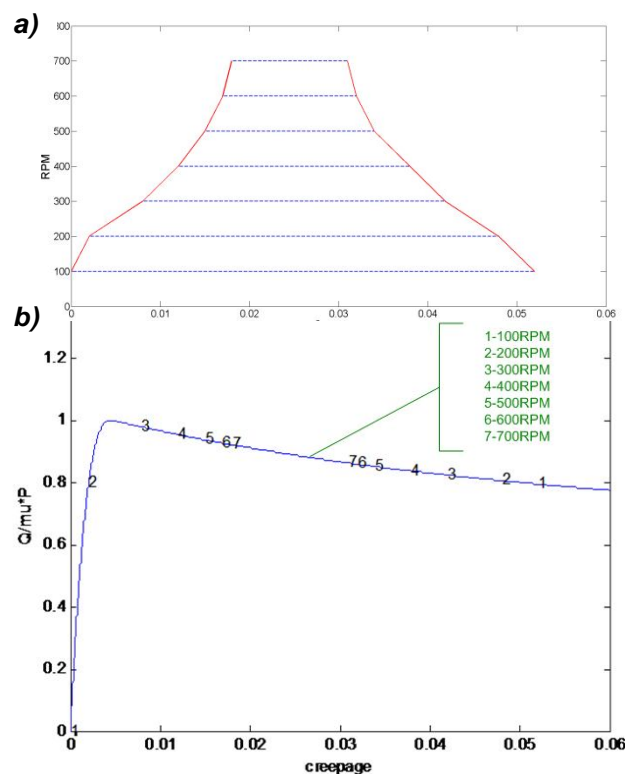


Figure 10. The creepage oscillation range at different rotation speeds for the 1138Hz mode during squeal.

In particular, Figure 10a) shows that as the testrig speed increases the creepage variation decreases. This is most likely because as the mean speed increases, the component of angle of attack due to lateral vibration of the wheel (\dot{y}/v_r) decreases. Figure 10b), alternatively shows the maximum and minimum creep variations for 7 different speeds from 100-700 RPM plotted on the traction-creep curve. These results additionally highlight that large nonlinear lateral creep and traction oscillations occur during squeal with an amplitude dependent upon the running speed. These large nonlinear (non-sinusoidal) amplitudes cause harmonics in the spectra of vibration and SPL as found in the testrig results of Figure 6.

5. CONCLUSION

A comprehensive analysis for prediction and validation of the modes of squeal vibration on a two disk testrig has been performed. In particular, a theoretical calculation based on a simplified geometry of the testrig disk, a finite element analysis based on the full geometry and experimental impact hammer tests performed on the testrig under static conditions have been used to predict squeal frequencies and modeshapes. Results for squeal frequencies have good correlation with actual dominant squeal noise frequency measurements under rolling conditions confirming the utility of the theoretical and experimental methods. Relatively small prediction errors in theoretical methods appear to be associated with imperfect modelling of the wheel geometry. In addition, an extra low frequency mode of vibration around 100Hz and associated equally spaced harmonics were found in the testrig squeal measurements that are likely due to shaft and/or bearings imperfections excited by the contact mechanics.

The occurrence of these frequency harmonics in the noise spectra was confirmed and investigated further using classical squeal modelling coupled with nonlinear contact mechanics. The model used was based on a classical, single mode/degree of freedom system coupled to a nonlinear lateral creep model for the rolling contact mechanics between the wheels. A numerical analysis of the contact dynamics was performed, to reveal model predicted harmonics correlating with those found in the sound spectra. These were shown to be due to nonlinear, large amplitude, creep oscillations. The effect of speed on the occurrence and characteristics of the harmonics was also investigated both theoretically and experimentally to reveal further insight into the nonlinear contact mechanical effects on squeal noise spectra. In particular, it was shown that increased running speed causes decreased nonlinear oscillations in creep, traction and vibration amplitudes.

The results provide strong evidence that the testrig squeal noise is primarily associated with transverse modes of vibration of the lower disk coupled with lateral creep oscillations at high AOA. In particular, the large oscillation lateral creep stick-slip phenomena is most likely to excite lateral/transverse modes of the largest most flexible wheel whose larger surface area is most efficient for converting lateral vibrations to pressure fluctuations in the air (ie sound waves). The nonlinear contact mechanics appears to cause a speed dependent filtering and/or amplifications of certain lateral squeal modes.

Further research should be directed towards investigation of the effect of different parameters

on the occurrence of testrig wheel squeal such as AOA, lubrication/friction modifiers, contact forces and humidity. It is noted that the simplified modelling of squeal is limited to providing theoretical insight that should be validated with further numerical, experimental and field investigations. For instance, the analysis does not take into account coupled vertical movement from the wheel profile at the contact point, coupled squeal modes due to the nonlinear creep model and non-stationary creep theory which may affect high frequency behaviour.

ACKNOWLEDGEMENTS

The authors are grateful to the CRC for Rail Innovation (established and supported under the Australian Government's Cooperative Research Centres program) for the funding of this research. Project No. R1.105 Improved Noise Management. The authors are very grateful for the support of the Rail CRC, RailCorp, Australian Rail Track Corporation PN and QR and all other members of the project steering committee including Uni. of Wollongong researchers, led by Dave Anderson.

REFERENCES

- 1 M.J. Rudd, *Whee/Rail noise – part II : Wheel Squeal*, Journal of Sound and Vibration (1976), 46 (3), p381-394.
- 2 P.J. Remington, *Wheel/Rail squeal and impact noise: What do we know? What don't we know? Where do we go from here?*, Journal of Sound and Vibration (1985), 116 (2), p339-353.
- 3 D.J. Thompson and C.J.C. Jones, *A review of the modelling of wheel/rail noise generation*, Journal of Sound and Vibration (2000), 231 (3), p519-536.
- 4 P.P. Kooijman, W.J. van Vliet, M.H.A. Janssens and F.G. de Beer 2000 Curve squeal of railbound vehicles (part 2): set-up for measurement of creepage dependent friction coefficient. Proceedings of Internoise, Nice, France, vol. 3, pp 1564-1567.
- 5 S. Descartes, C. Desrayaud, E. Niccolini and Y. Berthier, "Presence and role of the third body in a wheel-rail", *Wear*, 258(7-8), 2005, 1081-1090
- 6 M. Nakai, Y. Chiba, M. Yokoi, Railway wheel squeal (2nd report, mechanism of specific squeal frequency), *Bulletin of the JSME* 27 (224) (1984) 301-308.
- 7 M. Nakai, M. Yokoi, M. Sugiura, Railway wheel squeal (squeal of a rotating disk), *JSME International Journal, Series III* 32 (3) (1989) 406-412
- 8 M. Nakai, S. Akiyama, Railway wheel squeal (squeal of a disk subjected to periodic excitation), *Journal of Vibration and Acoustics* 120 (2) (1998) 614-622.
- 9 M.A. Heckl, I.D. Abrahams, Curve squeal of train wheels, part 1: mathematical model for its

- generation, *Journal of Sound and Vibration* 229 (3) (2000) 669–693.
- 10 M.A. Heckl, Curve squeal of train wheels, part 2: which wheel modes are prone to squeal? *Journal of Sound and Vibration* 229 (3) (2000) 695–707.
- 11 E. Schneider, K. Popp, H. Irrerier, Noise generation in railway wheels due to rail-wheel contact forces, *Journal of Sound and Vibration* 120 (2) (1988) 227–244.
- 12 U. Fingberg, A model of wheel-rail squealing noise, *Journal of Sound and Vibration* 143 (3) (1990) 365–377.
- 13 F.G. de Beer, M.H.A. Janssens, P.P. Kooijman, Squeal noise of rail-bound vehicles influenced by lateral contact position, *Journal of Sound and Vibration* 267 (3) (2003) 497–507.
- 14 J.F. Brunel, P. Dufre'noy, M. Nai' t, J.L. Mun' oz, F. Demilly, "Transient models for curve squeal noise", *Journal of Sound and Vibration* 293 (2006) 758–765.
- 15 D.T. Eadie, M. Santoro, "Top-of-rail friction control for curve noise mitigation and corrugation rate reduction", *Journal of Sound and Vibration* 293 (2006) 747–757
- 16 A.D. Monk-Steel, D.J. Thompson, F.G. de Beer, M.H.A. Janssens 2006 An investigation into the influence of longitudinal creepage on railway squeal noise due to lateral creepage. *Journal of Sound and Vibration* 293, pp 766-776.
- 17 Hsu, S.S., Huang, Z., Iwnicki, S.D., Thompson, D.J., Jones, C.J.C., Xie, G., Allen, P, "Experimental and theoretical investigation of railway wheel squeal" *Proceedings of the Institution of Mechanical Engineers, Part F (Journal of Rail and Rapid Transit)*, v 221, n F1, March 2007, p 59-73.
- 18 J.R. Koch, N. Vincent, H. Chollet, O. Chiello, "Curve squeal of urban rolling stock—Part 2: Parametric study on a 1/4 scale test rig", *Journal of Sound and Vibration* 293 (2006) 701–709
- 19 A. Jaschinski, H. Chollet, S. Iwnicki, A. Wickens, J. Würzen, The application of roller rigs to railway vehicle dynamics, *Vehicle System Dynamics* 31 (1999) 709 345–392.
- 20 P.A. Bellette, P.A. Meehan and W.J.T. Daniel, "Validation of a tangent track corrugation model with a two disk test rig", To appear in *Wear* doi:10.1016/j.wear.2010.10.020
- 21 Blevins and R.D., *Formulas for Natural Frequency and Mode Shape*. New York: Van Nostrand Reinhold Company, 1979.
- 22 Vogel, et al., "Natural Frequencies of Transversely Vibrating Uniform Annular Plates," *Appl.Mech.*, vol. 32, pp. 926-931, 1965.
- 23 Rao, et al., "Vibrations of Annular Plates Including the Effects of Rotary Inertia and Transverse Shear Deformation," *Sound Vib.*, vol. 42, pp. 305-324, 1975.
- 24 Daniel, et al., "Modelling the effects of Friction Modifiers on Rail corrugation in cornering," *Vehicle System Dynamics*, vol. 46, pp. 845-866, 2008.
- 25 Polach and O., "creep forces in simulations of traction vehicles running on adhesion limit," presented at the Proc. 6th International Conference on Contact Mechanics and Wear of Rail/Wheel Systems (CM2003), Gothenburg, Sweden, 2003.
- 26 Nielson and J.B., *New Developments in the Theory of Wheel/Rail Contact Mechanics*, . Lyngby, Danmark: Danmarks Tekniske Univeristyt, 1998.